Interaction Between Ruthenium Oxide Surfaces and Water Molecules. Effect of Surface Morphology and Water Coverage

Javier Heras-Domingo, Mariona Sodupe, Xavier Solans-Monfort*

Departament de Química, Universitat Autònoma de Barcelona (UAB), Cerdanyola del Vallès (Bellaterra), Spain 08193

Abstract

RuO_2 is a conducting transition metal oxide that has unique redox properties to be used as heterogeneous catalyst for oxidation reactions as well as in electrocatalysis. Furthermore, it has been reported to be an excellent catalyst for the oxygen evolution reaction, a key step for obtaining energy from water through environmentally friendly processes. In this context, a detailed knowledge of the RuO_2-water interface is important for a better understanding of the electrochemical process, the water oxidation reaction and some oxidative reactions involving RuO_2. Here, we use periodic boundary condition DFT (PBE-D2) calculations to analyze the influence of the surface morphology and water coverage in the adsorption energies and degree of water deprotonation. We have considered the four non-polar ((110), (011), (100) and (001)) most relevant surfaces and three degrees of water coverage: isolated molecules, half monolayer and full monolayer. Results indicate that three effects are crucial for determining the adsorption energy and degree of deprotonation: i) the intrinsic acidity of the unsaturated ruthenium cations and the intrinsic basicity of the O_{br} centers; ii) the presence of strong cooperative effects, already observed in the half monolayer situation of the (110) and (011) surfaces that favors 50% of deprotonation and leads to the formation of the $(H_3O_2)^-$ dimer; and iii) an increase of the surface basicity by the adsorption of water molecules on Ru centers bonded to O_{br} groups, which is more important in the (100) and (001) surfaces.

Introduction

RuO_2 is a conducting transition metal oxide that presents a rutile type structure as exclusively stable solid phase.[1,2] It has unique redox properties to be used as heterogeneous catalyst for oxidation reactions.[3–9] Moreover, it is an excellent material for electrocatalysis due to its high conductivity.[1,10–14] A selected list of the oxidation reactions that RuO_2 is able to catalyze includes CO, NH_3 and methanol oxidations, water formation and the Deacon process in which Cl_2 is formed from the oxidation of HCl.[1,3–7,15–17] In electrocatalysis, RuO_2 is used as anode in the chlor-alkali industrial process which forms Cl_2 and NaOH.[10,18] More recently, it has been shown to catalyze the hydrogen and the oxygen evolution reactions, which are key processes in the design of sustainable energy sources alternative to fossil fuels.[11–14]

The electrochemical processes involve solid – liquid (water) interfaces, which determines the nature of the active species.[1] The study of RuO_2 - water interaction is also relevant to understand the catalytic activity of hydrous RuO_2 (RuO_2-xH_2O)[19,20] as well as the origin of poisoning induced by water in the oxidation of CO.[21] Indeed, in the last decades, considerable efforts have been devoted to study - water metal oxide interfaces[9,22–27] due to their relevance in many scientific fields such as catalysis, electrochemistry, corrosion, geology, or atmospheric science.[28–31] For the particular case of RuO_2, most of the existing studies focus on the most stable (110) surface, which is characterized by the presence of unsaturated pentacoordinated ruthenium atoms (Ru_{5C}) and bridged oxygens (O_{br}) (Figure 1).

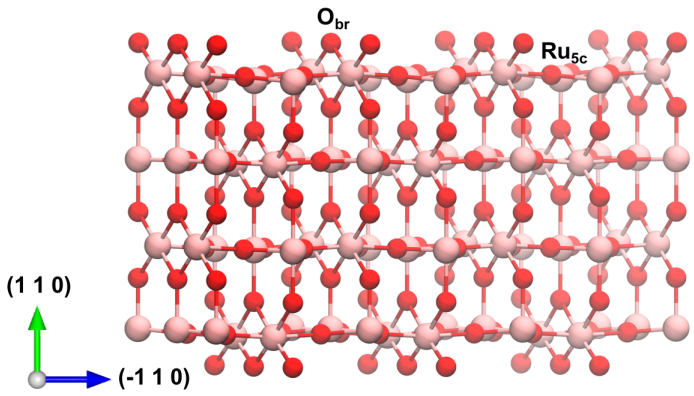

Figure 1. Defect free RuO_2 (110) surface.

The water – oxide interface has been studied by using several spectroscopic techniques such as X-ray scattering measurements, High-resolution electron energy loss spectroscopy (HREELS) and thermal desorption spectroscopy (TDS). It has also been studied by means of scanning tunneling microscopy (STM) and DFT calculations.[32–41] It is found that the interface nature highly depends on the experimental conditions, particularly on the applied voltage. Regarding studies without the addition of other species or external voltages, Lobo and Conrad concluded, from HREELS and TDS spectroscopies, that adsorption mainly involves non-dissociated water molecules.[32] These molecules are located at Ru_{5C} centers and stablish hydrogen bond interactions with O_{br} oxygens. Furthermore, water molecules desorb at around 400 K, which is consistent with a water adsorption energy of about -96 kJ mol^{-1}. Similar adsorption energies were obtained by means of DFT by Siahrostami and Vojvodic, although they suggested that H_2O on RuO_2 is prone to dissociate.[39] More recently, Dohnálek and co-workers combined STM microscopy and DFT calculations and analyzed the effect of water coverage on the (110) RuO_2 surface.[27,35–37] They showed that at very low coverages, single water adsorbs on Ru_{5C} centers and that the Ru_{5C}-H_2O is in equilibrium with the deprotonated Ru_{5C}-OH···H-O_{br} species, as a result of the Lewis acidity of

the ruthenium atoms. This study also shows that increasing the water coverage allows the formation of water dimers. The two water molecules of these dimers are adsorbed in contiguous Ru_{5C} centers and one of them is deprotonated, which leads to the formation of the $H_3O_2^-$ motif. At even higher water coverages, hydrogen bonded chains of water molecules are formed. These chains are characterized by the presence of the same $(H_3O_2^-)_n$ motif, which constitutes the fundamental building block. Computed adsorption energies per water molecule vary from -121 to -146 kJ mol^{-1}, depending on the amount of water and the degree of deprotonation.[34–36,39,40]

At this point it is worth noting that, to the best of our knowledge, the adsorption of water molecules at different surfaces, besides the most stable (110) one, have not been addressed before. Only very recently during the revision process a combined experimental and computational work appeared in the literature. In this work, authors studied the interface between water and all relevant surfaces of RuO_2 and they concluded that the degree of water deprotonation is higher for the (011) surface followed by the (110), the (001) and finally the (100).[42]. Thus, with the aim of analyzing how the surface morphology and the water coverage influence the H_2O-RuO_2 interface, present work analyzes the interaction of water molecules, starting from one molecule to a full monolayer, on the main crystallographic orientations (110), (100), (011) and (001) of flawless RuO_2 surfaces. For that, we use periodic boundary DFT calculations and we focus on the degree of water deprotonation as a function of the surface topology, surface electronic structure and water coverage.

Computational details

Calculations were carried out using density functional theory (DFT)[43] with periodic boundary conditions as implemented the *Vienna Ab Initio Simulation Package* (VASP) code.[44,45] All calculations were performed considering the projector augmented wave (PAW) pseudopotentials.[46,47] The external electrons were expanded in plane waves with kinetic energy cut-off equal to 500 eV. The chosen functional was the PBE exchange correlation GGA functional.[48] This functional is the most commonly used for studying RuO_2 and correctly describes its conducting nature.[8,34–37,39,42,49,50] The D2 Grimme's dispersion correction was included in all the slab calculations since it is essential to properly describe water adsorption and hydrogen bonding.[51] Test calculations with the most recent D3 approach were also performed with the aim of analyzing the influence of the Grimme's parametrization in the adsorption energies and the relative stabilities between the H_2O and the OH^-/H^+ deprotonated structures. Results are summarized in Table SX of the supporting information. They show that D3 parametrization marginally reduces the adsorption energy by less than 2.6 kJ mol^{-1}. However, this diminution of the adsorption energy is very similar for the two forms (H_2O or OH^-/H^+). Therefore, this leads to the same relative stability between the two forms regardless the Grimme's parametrizations. Bulk calculations were performed considering a K-point mesh for the Brillouin zone (BZ) of (15,15,15) employing the Monkhorst-Pack grid (MP),[52] while slab calculations were performed considering a Monkhorst-Pack K-point mesh of (6,6,1). The cut-off and K-point mesh were calibrated by ensuring the convergence of both cell parameters and cell energies. (*Supporting Information S1- S2)*. The energy convergence criteria was fixed to 10^{-5} and 10^{-4} eV for electronic and geometry relaxations, respectively.

Surface models of the main crystallographic orientations were built by cutting out the slab from the optimized bulk structure, with the MOLDRAW graphic program.[53] The considered slabs were constructed considering a (2x1) supercell and a 4-layer thickness, the minimum slab

thickness for a surface energy convergence (*Supporting Information S3)*. The c value was set to 35 Å ensuring an interlayer distance of at least 21 Å to minimize the interaction between replicas at the *(h k l)* perpendicular direction. The size of the models was large enough to represent the main properties and atoms positions were fully relaxed. Surface energies of the different facets were computed through the following equation:

$$\gamma_{(hkl)} = \frac{E_{slab} - (N \cdot E_{bulk})}{2 \cdot A} \qquad (1)$$

where E_{slab} is the energy corresponding to the relaxed surface without optimizing the bulk cell parameters; E_{bulk} is the fully relaxed bulk energy; N is the number of formula units in the slab per units in the bulk unit cell, and (2A) the corresponding two cross-section area of the slab.

Water adsorption on the surfaces at different coverages was studied by varying the number of water molecules per unit cell from one to four for surfaces (110), (100) and (001) and from one to eight for the (011) facet. In both cases, the largest number of water molecules corresponds to a water monolayer on the surface. Two type of water adsorption energies are reported along the text. The adsorption energy per water molecule, which is calculated through the following equation:

$$E_{ads} = \frac{E_{(hkl)+H_2O} - E_{(hkl)} - (n_{H_2O} \cdot E_{H_2O})}{n_{H_2O}} \qquad (2)$$

where the $E_{(hkl)+H2O}$ is the total energy of the slab with the already adsorbed water, $E_{(hkl)}$ is the total energy of the slab model, E_{H2O} the total energy of an isolated water inside a 15x15x15 $Å^3$ cubic

box and $n_{(H2O)}$ the number of adsorbed waters onto the surfaces. The adsorption energy per surface are, which is calculated through equation 3:

$$E_{ads/A} = \frac{E_{(hkl)+H_2O} - E_{(hkl)} - (n_{H_2O} \cdot E_{H_2O})}{A} \quad (3)$$

Where all terms are equal to those of equation 2 except A, which stands for the surface area of the supercell.

At this point it is worth mentioning that test calculations including additional water through the implicit PCM continuum model were performed on the adsorption of a single water molecule either deprotonated or not on the (110) and (100) surfaces as well as the most favorable monolayer structures with the aim of evaluating the effect of solvent. Results are reported in Table SX of the Supporting Information. They show that inclusion of additional water with a continuum model produce an important decrease of the global adsorption energy of about 27 to 39 kJ mol^{-1} for both the H_2O and OH^-/H^+ forms. For the adsorption of a single water molecule, the decrease in the adsorption energy is larger for the form in which water is deprotonated, thus the preference for the deprotonated form in the (110) surface (see below) is reduced, while the preference for the non-deprotonated form is larger in the (100) (see below). The diminution of the E_{ads} when using PCM is also observed for the monolayer structures. However, the differences between the two analyzed structures are smaller and thus the relative stabilities between them remain almost unaltered. Therefore, although the absolute values reported along the text may be slightly overestimated, we do not expect that describing additional water through a continuum model will change the major trends reported in this study

Transition state geometries (TS) and energy barriers (ΔE) were studied through the climbing image nudged elastic band (CI-NEB)[54,55] method, as implemented in the VASP Transition

State Tools (VTST) code. The climbing image variation was used in order to converge onto the saddle point and explore the minimum energy path (MEP). For that, we used 4 images between reagents and products and the Quick-Min algorithm as optimizer.[56] As a convergence criteria, the maximum force at any atom in every image was required to be below the 0.05 eV/Å threshold. Transition states were finally verified by the presence of a single imaginary frequency through the harmonic vibrational analysis.

Results and Discussion

Results are divided into four subsections. First, we focus on the properties of RuO_2 main crystallographic surfaces. Then, we address the adsorption of one single water molecule at each surface, with the main goal of understanding the intrinsic interaction between water and RuO_2 facets. In the third subsection, we analyze the influence of cooperative effects on the water adsorption energies and on the degree of deprotonation at each surface, by analyzing the half monolayer coverage, which is associated with the formation of water chains[35,36] (see below). Finally, we focus on the structure of the water monolayer in each surface and analyze the factors that determine this structure. In this section, we report the adsorption energies per surface area, which allows considering the density of adsorbed molecules in each surface. This is used to obtain the Wulff construction of a nanoparticle growth in thermodynamic equilibrium in water solution.

Ruthenium Oxide bulk and surfaces. RuO_2 crystallizes in a rutile-structure with space group $P4_2/mmm$, where Ru^{4+} exhibits a distorted octahedral coordination with four long Ru-O distances in the equatorial plane and two short Ru-O ones in the axial position.[57,58] The oxygen atom displays a trigonal planar environment, with two long and one short Ru-O distances. The optimization of

the bulk crystal structure of RuO_2 led to the following lattice parameters *a=b=4.54 Å, c=3.13* and $\alpha=\beta=\gamma=90^o$, the Ru-O distances being 1.996 Å and 1.945 Å for equatorial and axial oxygens, respectively (Bold values in Table S2 of the Supporting Information). The computed data are in good agreement with the experimental measurements for cell parameters (*a=b=4.4910 ± 0.0004 Å, c=3.13± 0.0004 Å* and $\alpha=\beta=\gamma=90^o$) and for Ru-O equatorial and axial distances (1.984 and 1.942 Å).[57,58]

The full optimized unit cell was used to build the slab models of each crystallographic orientation, which are represented in Figure 2. The (110) and (011) facets have at the outermost layer two coordinated bridging oxygen O_{br} and 5-coordinated Ru_{5c} atoms. It is worth pointing out that the Ru_{5C} centers of (110) and (011) surfaces differ on the nature of the vacant site. The vacant site in the Ru_{5C} center of the (110) surface is axial, while that of the (011) surface is equatorial. The surface (100) exhibits a saw morphology, with 2-coordinated oxygen atoms (O_{2c}) and 3-coordinated O_{3c} bonded to 5-coordianted Ru_{5c} atoms, with the vacant site in axial position. Finally, the (001) facet displays all Ru atoms as a 4-coordinated Ru_{4c} and all the oxygen atoms as 2-coordinated O_{2c}, the vacant sites of Ru_{4C} centers being both equatorial.

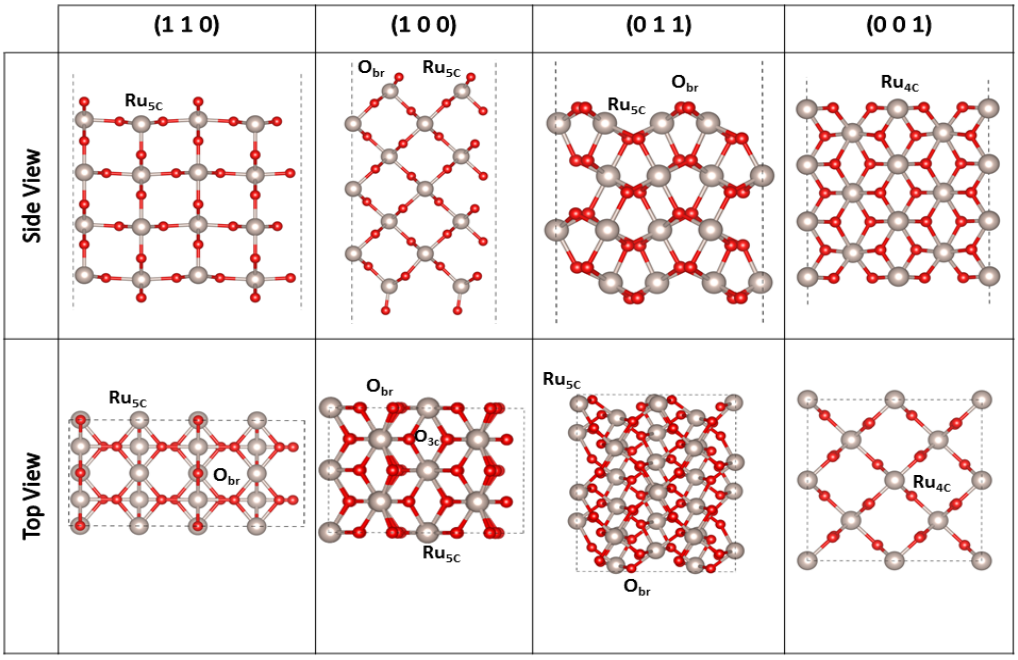

Figure 2. *crystallographic surface models used in this work*

The Ru-O distances of outermost layer of the different slabs, the Bader charges of the oxygen bridge (O_{br}) and unsaturated ruthenium atoms Ru_{CUS}, as well as the computed surface energies are given in Table 1. This table also includes the values of the bulk for comparison. Regardless of the slab orientation, the internal 6-coordinated Ru_{6c} atoms present Ru-O distances (1.90 – 2.05Å) that are close to the bulk values and are not discussed further. Regarding the surface atoms, the Ru-O distances vary depending on the coordination environment, the strongest bonds corresponding, as expected, to 4-coordinated Ru_{4c} atoms, present at the (001) surface. Indeed, the 5-coordinated Ru_{5c}, present at the (110), (100) and (011) surfaces, show significantly larger bond distances (average values ranging 1.96-1.97 Å compared with 1.89 Å for the (001) surface). Remarkably, the distance between unsaturated Ru-centers at the surface varies significantly from one surface to another. The shortest distances (3.173Å) are found for the (110) and (100) surfaces, while the Ru-Ru distances in the (001) surface are significantly larger (4.543Å).

Table 1. *Computed surface energies ($\gamma_{(hkl)}$) and Ru-O distances of the outermost layer of the main crystallographic orientations. Surface energies are in eV/Å² and distances in Å.*

(h k l)	$\gamma_{(hkl)}$	$d(Ru\text{-}O)_{eq}$	$d(Ru\text{-}O)_{ax.}$	d(Ru···Ru).	q_{Ru}[a]	q_O[a]
Bulk	--	1.996	1.945	3.137		
(1 1 0)	0.066	1.995	1.880	3.137	+1.60	-0.75
(0 1 1)	0.074	1.873-2.111	1.948	3.735	+1.64	-0.78
(1 0 0)	0.082	1.926-2.032	1.901	3.137	+1.65	-0.75
(0 0 1)	0.099	1.923	1.849	4.543	+1.54	-0.81

[a] Bader atomic charges of the Ru and O unsaturated atoms of the surface

The surface energies of all stoichiometric orientations are similar to previous values reported in the literature.[1,59–62] These values are used to get the equilibrium shape of a crystal (under vacuum conditions) through the Wulff construction approach,[63] plotted with a python library called pymatgen[64] (Figure 3). The Wulff construction is obtained by minimizing the global surface energy of the nanoparticle – medium interface, which implies that the lowest the surface energy of a facet is, the largest contribution it has in the equilibrium structure of a given material. In our case, the surface families with lower surface energies are the (1 1 0) and the (0 1 1) ones, which account for the 43.6% and 49.2%, respectively, of the total surface area (see Figure 3). Note that the (011) family present a higher contribution than the (110) one despite the higher surface energy of the former. This is associated to the fact that there are eight equivalent orientations of the (011) given by symmetry, while the (110) family only has four equivalent planes. Surfaces equivalent to the (100) facet slash the edge between the (110) family surfaces and account for a 7.2%. Finally, the (001) facet, with the highest surface energy has a negligible contribution to the equilibrium shape.

Remarkably, these contributions are in good agreement with experimental observations in single crystals grown by deposition from the vapor face through a process in which only the constituents of ruthenium oxides are in the reactor. The available data show that the (011) is the predominant facet followed by the (100) and (110) ones.[1]

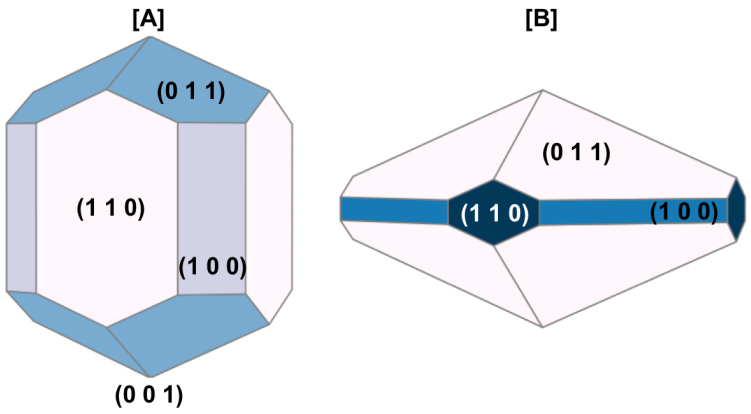

Figure 3. *Ruthenium Oxide Wulff construction obtained with the here computed surface energies in gas phase and solution (assuming a monolayer coverage).*

Adsorption of isolated water molecules at the different RuO_2 surfaces (θ= 1/4 or 1/8). A water molecule was adsorbed on to the clean surfaces with the aim of studying the intrinsic interactions between water and RuO_2 surfaces as a function of the surface topology. This corresponds to a water coverage of 1/4 for surfaces (110), (100) and (001) and a coverage of 1/8 for the (011) facet. We considered the adsorption of the water molecule in both the non-deprotonated and the deprotonated forms. These two situations will be hereafter referred to *wat* and *dpro,* respectively. We also located the transition structure connecting both minima through the image climbing nudged elastic band (CI-NEB) method.[54,55] The relative energies, the major structural parameters associated to this coverage and the Bader charges of the unsaturated Ru and

O atoms of the surface and the adsorbed water molecule are given in Table 2. Further details about the optimized structures are given in the Supporting Information (*Section S4)*.

In all considered surfaces, at least two different minima are found. One of these minima corresponds to the adsorption of water, the other is related with the formation of OH^-/H^+ pairs through water deprotonation. Regardless the surface morphology, the adsorbed water molecule interacts directly through its oxygen with the under-coordinated Ru_{4c} and Ru_{5c} to fill the empty coordination sites. Besides, a quite strong hydrogen bonding between one H atom of the water molecule and the nearest bridged oxygen O_{br} is also formed. The $Ru\cdots O_{wat}$ distances are similar in all surfaces and they range from 2.172 to 2.180. Larger differences are observed for the $H_{wat}\cdots O_{br}$ distances, the values varying between 1.588 and 1.688 Å. The $H\cdots O_{br}$ distance seems to be related with the surface morphology and in particular the distance between Ru_{5C} and O_{br}. Indeed, the shortest $H\cdots O_{br}$ distances tend to be associated with the smallest separation between the Ru_{5C} and O_{br} centers. In the (001) surface, the water molecule establishes two hydrogen bonds with the closest O_{br} atoms in a bifurcated manner. Remarkably, another adduct with only one H-bond has also been located. This additional structure is less stable than that with two H-bonds by 17.1 kJ mol^{-1}.

The water adsorption energy at the different surfaces ranges between -115.4 to -133.8 kJ mol^{-1}. The weakest adsorption (E_{ads} = -115.4 kJ mol^{-1}) corresponds to the (011) surface. In the other three surfaces the adsorption energy is significantly larger, ranging from -129.2 to -132.8 kJ mol^{-1}. This stronger interaction of water with the (110), (100) and (001) surfaces is related to the number and strength of the $H\cdots O_{br}$ hydrogen bonds, which in turn depends on the morphology of the surface.

With the aim of further analyzing the intrinsic interaction between H_2O and RuO_2 surfaces, we computed the Bader atomic charges (Table 2) and analyzed the density of states (DOS) of the clean surface and the *wat* and *dpro* structures. Figure 4 shows the contribution to the DOS of the 4d orbitals of the unsaturated ruthenium center in which water is adsorbed, that of the p orbitals of the oxygen bridge receiving the proton in the *dpro* structure and that of the p orbitals of the oxygen of the water molecule. Bader atomic charges shows that interaction between H_2O and the surface produce some electron transfer from the water molecule to the surface. Interestingly, this electron density does not accumulate on the Ru center (that becomes even more positively charged with respect to the clean surface (Table 1)) but the oxygen atoms of the surface and particularly the oxygen bridge. This agrees with the DOS which shows that the interaction between water and the RuO_2 surface is stablished within an occupied p orbital of water and an empty d orbital of ruthenium (Figure SX of the supporting information). Remarkably, when comparing the contributions of the oxygen bridge p orbitals in the DOS of the different clean surfaces (Figure 4), it is observed that in the (110) surface the p orbital involved in the hydrogen bonding with water is at higher energies, thus suggesting higher basicity. Overall three key factors are identified: i) the smallest the separation between the Ru_{5C} and the O_{br}, the shortest the $H\cdots O_{br}$ distance and the strongest the H-bond; ii) the higher basicity of the O_{br} sites in the (110) and (100) surfaces, the larger the strength of the $H\cdots O_{br}$ H-bond; and iii) the presence of two hydrogen bonds in the case of the (001) surface also increases the adsorption energy.

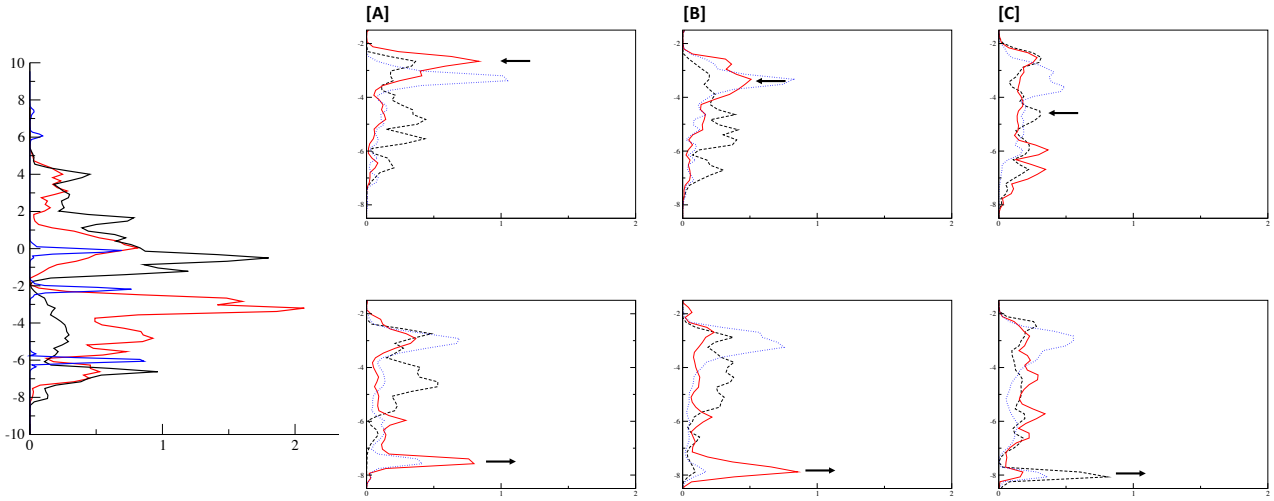

Figure 4. *Projected density of states (pDOS) of the (110) clean surface including the pDOS of the isolated water molecule (Left). The black line corresponds to the 4d Ru_{5C} orbitals, the red lined are the 2p orbitals of Obr and the blue one the orbitals of water. On the right the pDOS associated to the 2p orbitals of OBr in the clean surfaces (top) and in dpro structures (bottom) are reported: [a] (110) surface; [b] (100) and [c] (011). The red solid line 2py, the blue doted line 2pz and dashed black line 2px.*

Table 2. *Water adsorption energies on the most favorable facets (kJ mol^{-1}) at low water coverage θ=(1/4 or 1/8) and the associated main structural parameters (Å).*

(h k l)		E_{ads}	O_w-H_w	O_{br}-H_w	Ru-O_w	q_{Ru}[a]	q_O[a]	q_{H2O}
	wat	-131.3	1.038	1.588	2.172	+1.67	-0.87	+0.10
(1 1 0)	*TS*	-128.3	1.212	1.252	2.106			
	dpro	-139.6	1.754	1.011	1.993	+1.68	-1.08	-0.46/+0.66
	wat	-115.4	1.021	1.615	2.177	+1.73	-0.89	+0.10
(0 1 1)	*TS*	-104.5	1.317	1.137	2.059			
	Dpro	-102.8	1.429	1.072	2.031	+1.79	-1.04	-0.49/+0.64
	Wat	-129.2	1.013	1.688	2.180	+1.70	-0.87	+0.10
(1 0 0)	*TS*	-111.6	1.333	1.136	2.074			
	Dpro	-114.5	1.548	1.044	2.032	+1.76	-1.05	-0.46/+0.60
(0 0 1)	*Wat*	-133.8	1.018	1.627 1.627	2.172	+1.62	-0.93	+0.07

[a] Bader atomic charges of the Ru and O unsaturated atoms of the surface

Structures in which water dissociates upon adsorption on RuO_2 show that the proton transfer toward O_{br} decreases the Ru-O_w distance by around 0.1 and 0.2 Å, as a result of the larger OH^- basicity compared to that of H_2O. Similarly, the O_{br}-Ru bond distance of the surface increases due to a decrease of the O_{br} basicity upon protonation (values ranging from 1.982 to 2.090 Å). Besides, the H^+ and OH^- moieties interact through hydrogen bonding. The $H_{br}\cdots O_W$ distance varies from 1.377 to 1.754 Å, indicating that the H-bond is stronger in the *dprot* structure than in the *wat* one with the exception of the (110) surface. Regarding the energetics, calculations indicate that deprotonation is a favorable process (ΔE = -8.3 kJ/mol) only in the case of the (110) surface, reaction energies at the (100), (011) and (001) surfaces being +14.6, +12.5 and +24.7 kJ mol^{-1} respectively. Remarkably, the thermodynamics of water deprotonation correlate well with the Ru-O_w distance after deprotonation. Indeed, the shortest Ru-O_w distance (1.993 Å) is found for the (110) surface, intermediate values (2.031-2.032) are obtained for the (100) and (011) facets and the longest distance is found for the (001) surface (2.066 Å). Furthermore, the basicity of O_{br} is expected to be larger in the case of the (110) surface. This can be related to three factors: the p orbital capturing the proton lies at higher energies in the (110) surface than the others (Figure 4), the Bader charge on the O_{br} upon protonation becomes more negative than in the other surface and iii) the Ru-O-Ru angle is smaller which it is usually associated with an increase of the basicity. Therefore, the water deprotonation thermodynamics does not seem to be related with the strength of the H-bonding formed between the H^+ and OH^- moieties but with the interaction of these two fragments with the surface. That is, surface deformation energy upon proton transfer is small for all facets and the geometry features suggest that both Ru-OH and O_{br}-H interactions are stronger for the (110) surface, the only one in which deprotonation is thermodynamically favorable.

The potential energy profiles corresponding to the water deprotonation process on the different surfaces are shown in Figure 5. Remarkably, in all cases, the energy barriers are low; i.e., they range from 2.9 kJ mol^{-1} for the (110) surface to 25.9 kJ mol^{-1} for the (001) one. Indeed, the lowest energy barrier is found for the thermodynamically preferred process (deprotonation on the (110) facet), while the highest one corresponds to the less favorable one (the (001) surface). For this latter surface, water deprotonation occurs from the *wat* structure presenting one single H-bond with O_{br} atoms of the surface.[65] This structure is less stable than the one with two hydrogen bonds by 17.1 kJ mol^{-1}. Therefore, most of the energy required for the water deprotonation arise from changing the coordination mode of the water molecule.

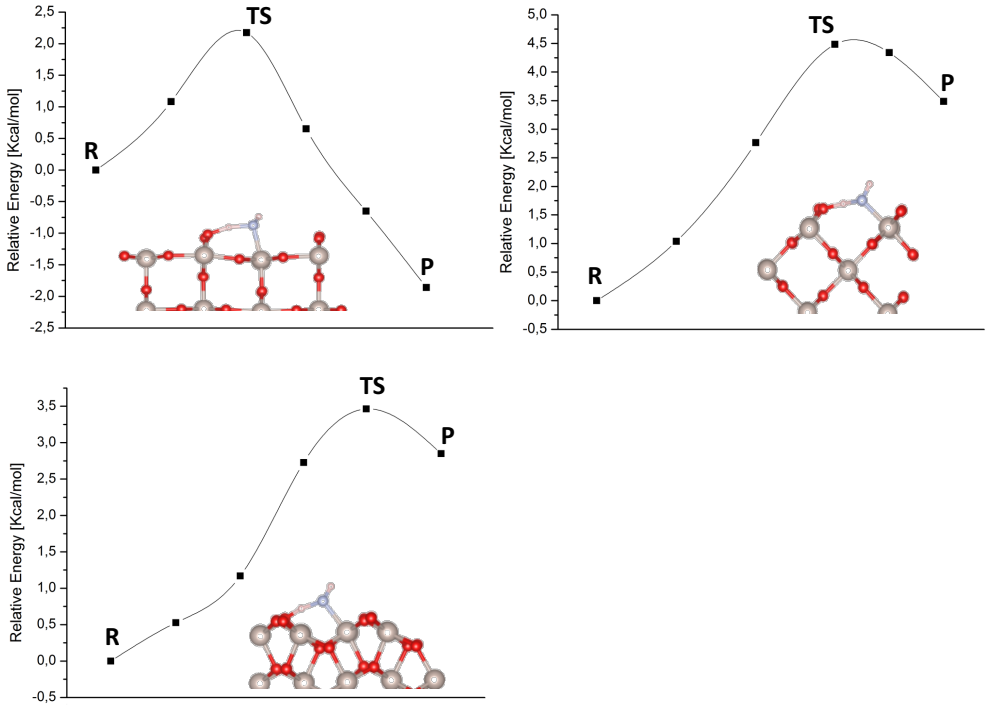

Figure 5. *Energy profiles associated to the water deprotonation at low coverages on the different surfaces.*

In summary, at low water coverage (θ=1/4 and (θ=1/8), only the most stable (110) surface will exhibit deprotonation. Differences are related to the surface topology which influences the basicity of the O_{br} on each surface (see the associated DOS in Figure 4) and the interaction between the OH^- and the unsaturated ruthenium center. At higher water coverages, however, cooperative H-bond interactions could lower the energy requirements to decompose water on each orientation.

Water adsorption at the half monolayer coverage θ = (2/4). Significant differences are observed upon adsorption of a second water molecule to the (110), (100) and (001) surface as well as three additional water molecules to the (011) surface. In both cases, the water coverage is 1/2, that is, half of the initially unsaturated ruthenium atoms have a water molecule adsorbed. For each surface we explore at least three potential situations: a) no deprotonated water molecules (*wat/wat)*; b) half of the water molecules are deprotonated (*wat/dpro)*; and c) all water molecules are deprotonated (*dpro/dpro)*. Furthermore, with the aim of evaluating the cooperative effects (see below) for the case of the (110) and (001) facets, we also explored the possibility that the water molecules adsorb in the two closer Ru-centers (*-c*) or in two Ru-centers that are further separated (*-f*). Relative energies for both the non-deprotonated and deprotonated forms, as well as major structural parameters are given in Table 3. Figure 5 shows the optimized geometries of the structures associated to the (110) surface and Figure 6 presents the most stable structures associated to the other facets.

First of all, we focus on the (110) surface. Here we explore the adsorption on adjacent Ru atoms as well as the adsorption on Ru centers separated by the O_{br} chain. The adsorption of two water molecules in Ru centers separated by the O_{br} chain (distance between Ru centers is more than 6.3 Å) leads to an adsorption energy per water molecule that it is almost equal to that

computed for an isolated water molecule. The structural parameters are also very similar to those of the adsorption of a single water molecule and no H-bonding between the two water molecules is formed (Figure 5a). Similarly, the adsorption energy per water unit of two deprotonated water molecules in two distant Ru_{5C} centers is essentially that of a single deprotonated water molecule. Again, no hydrogen bonding between the two OH^-/H^+ fragments is stablished (Figure 5b). In this context, the adsorption of one water molecule and one OH^-/H^+ motive in distant Ru centers leads to an adsorption energy per H_2O unit that is in between the adsorption energy of one H_2O and that of a deprotonated water molecule (Supporting Information section S5).

Table 3. *Water adsorption energies on the most favorable facets (in kJ mol^{-1}) at half monolayer coverages θ=(2/4 or 4/8) and the associated main structural parameters (in Å).*

(h k l)		**E_{ads}**	**Ru···Ru**	**O_{w1}-H_{w1}**	**O_{br}-H_{w1}**	**O_{br}-H_{w2}**	**Ru-O_{w1}**	**Ru-O_{w2}**	**O_{w1}-H_{w2}**
(1 1 0)	*wat/wat-c*[a]	-142.5	3.138	1.384	1.605	1.650	2.226	2.222	2.298
	wat/dpro-c[a]	-151.3	3.149	1.920	0.999	1.846	2.044	2.198	1.739
	dpro/dpro-c[a]	-149.6	3.139	1.864	1.005	1.009	2.002	2.002	2.234
	wat/wat-f[b]	-131.7	6.380	1.030	1.662	1.689	2.203	2.204	---
	wat/dpro-f[b]	-139.2	6.427	1.765	1.010	1.606	1.996	2.181	---
	dpro/dpro-f[b]	-143.0	6.426	1.782	1.008	1.007	1.990	1.989	---
(0 1 1)	*4wat*	-126.7	3.666	0.974	1.022	3.035	2.097	2.202	1.463
	2wat/2dpro	-132.1	3.679	0.974	1.022	3.536	2.093	2.166	1.494
	1wat/3dpro	-127.5	3.674	0.975	1.023	3.530	2.092	2.207	1.481
(1 0 0)	*wat/wat*	-128.3	3.144	1.007	1.711	1.676	2.204	2.204	2.346
	wat/dpro	-127.1	3.069	1.603	1.044	2.233	2.073	2.179	1.717
	dpro/dpro	-112.9	3.081	0.977	1.016	1.023	2.012	2.027	2.275

	wat/wat-c[a]	-126.2	4.554	0.975	1.535	1.711	2.186	2.168	--
(0 0 1)	*wat/dpro-c*[a]	-122.9	4.483	0.975	1.077	1.673	2.052	2.167	--
	wat/wat-f[b]	-122.4	6.402	1.039	1.519	1.643	2.185	2.165	2.952

[a] Water adsorption takes place in adjacent unsaturated ruthenium centers.

[b] Water adsorption takes place in distant unsaturated ruthenium centers.

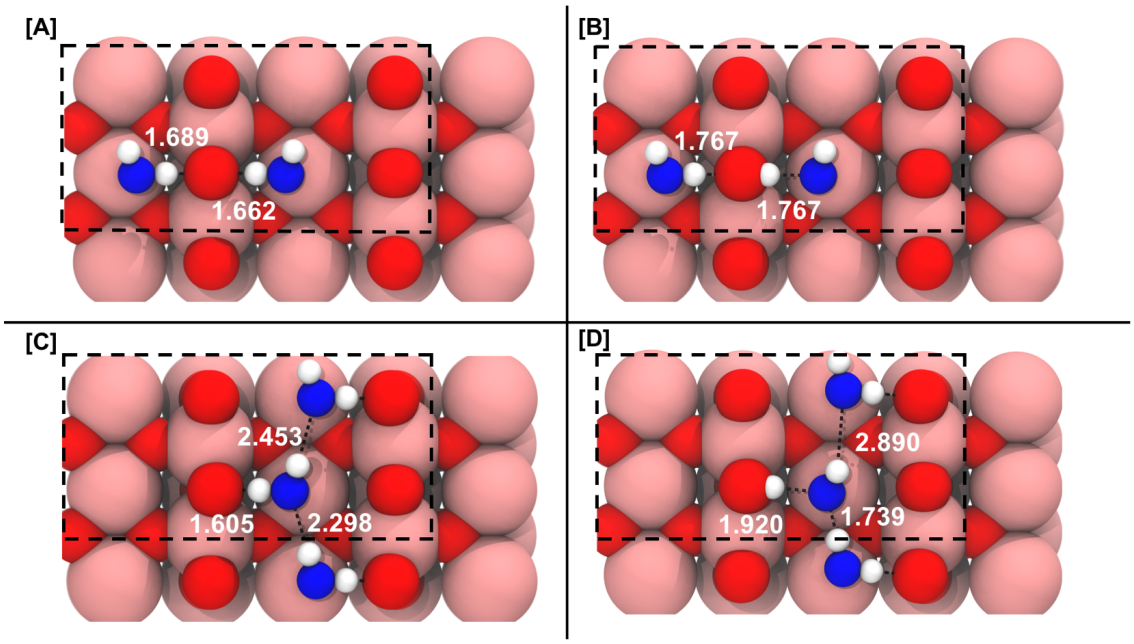

Figure 6. *Optimized structures associated to water adsorption on the (110) surface with a half monolayer coverage (θ = 2/4). The four resulting structures are: a) wat/wat-f; b) wat/dpro-f, c) wat/wat-c and d) wat/dpro-c. Distances are in Å*

The situation is completely different when the adsorption takes place on contiguous ruthenium centers (the distance between Ru centers in the pristine surface is 3.137 Å). The adsorption of two water molecules leads to an adsorption energy per water molecule of -142.5 kJ mol^{-1}, which is larger (in absolute value) than that determined for the adsorption of one water molecule (-131.3 kJ mol^{-1}). This indicates the presence of cooperative effects as a result of moderate hydrogen bond interactions between water molecules, the $H_{w1}\cdots O_{w2}$ distance being 2.298

Å (Figure 5c). Note that, the structural parameters associated with the Ru···H_2O interaction are similar to those of the isolated water and the subtle differences suggest that the interaction between the RuO_2 surface and the adsorbed molecules is weaker at higher coverages (larger Ru_{5C}···O_w and O_{Br}···H_w distances). Similarly, the formation of two OH^-/H^+ species on contiguous Ru centers leads to an adsorption energy that it is also higher than that of one isolated OH^-/H^+ species (-149.6 *vs.* 131.6 kJ mol^{-1}).[66] The origin of this extra stabilization arises again from the formation of moderate hydrogen bonding between OH^-/H^+ fragments (2.234 Å) rather than from a stronger interaction with the surface.

Finally, the situation in which one of the water molecules is deprotonated by a 2-coordinated bridged oxygen atom O_{br} of the oxide surface and the other remains as molecular water results in the formation of a formally $H_3O_2^-$ species (Figure 5d), with a strong intermolecular hydrogen bond (1.739 Å). In contrast, the H-bonding between the hydrogen atom of the OH^- fragment and the subsequent water molecule is significantly larger (2.890 Å). As a result, units formed by formally one OH^- and one H_2O molecule; i.e., $H_3O_2^-$ species, are clearly identified. At this point it should be highlighted that, as already observed for the OH^-/H^+ form, the Ru-OH interaction has an important covalent behavior, which produces a significant electron donation from the formal OH^- to the RuO_2 surface that accumulates on the oxygen atoms of the surface and particularly the O_{br}. Overall the negative charge on O_{br} significantly increases and the Bader charge of the formal $H_3O_2^-$ unit is significantly smaller than -1. In any case, for simplicity we will refer to the here described pattern as $H_3O_2^-$ species, even though its charge indicates an intermediate situation. The adsorption energy of -151.3 kJ mol^{-1} is larger than the adsorption of two water molecules, either in their neutral and deprotonated forms. Overall, calculations suggest that the

majority of adsorbed water molecules in the (110) surface are in the form of $H_3O_2^-$ dimers due to the strength of the cooperative effects as recently reported by Dohnálek and co-workers.[35,36]

The situation for the remaining surfaces is similar to that of the (110) facet, but with some particularities associated to the morphology of each surface. In the (011) facet, the contiguous unsaturated Ru_{5C} centers are still sufficiently close (3.731 Å in the clean surface) that cooperative effects between adsorbed water molecules, OH^-/H^+ species or combination of both are also present when four water molecules are adsorbed. This leads to an adsorption energy per water molecule that is higher than that of a single water (either in its neutral or deprotanated forms). Interestingly, stronger cooperative effects are again found when the formal $H_2O_3^-$ dimer is formed (Figure 6a). Because of that, structures such as *3wat/1dpro* or *4dpro* are not found as minima on the potential energy surface and evolve to *2wat/2dpro* and *1wat/3dpro* situations, respectively. Indeed, the gain achieved with the cooperative effects resulting from the formation of the $H_2O_3^-$ dimers are sufficient to compensate the 12.6 kJ mol^{-1} preference for the adsorption of molecular water with respect to water dissociation. Overall, the situation in which 50% of water molecules are deprotonated is preferred by 5.4 kJ mol^{-1}.

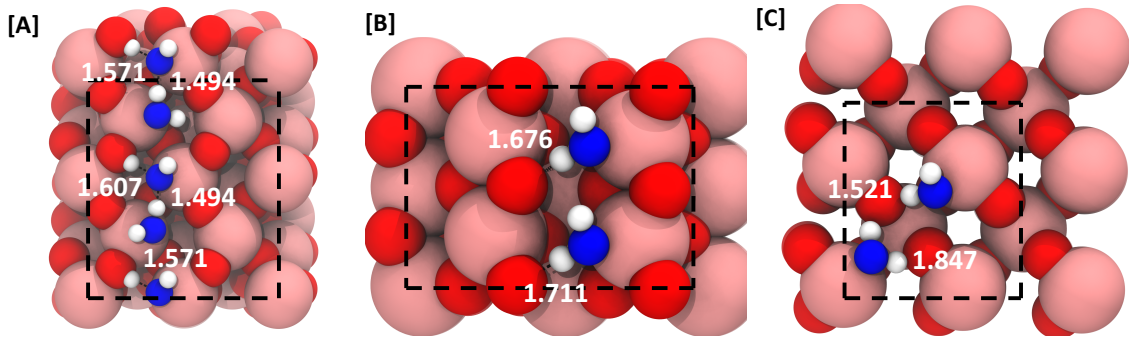

Figure 7. *Optimized geometries of the most stable structures associated to water adsorption with a half monolayer coverage (θ = 2/4 or 4/8) on the: a) (011); b) (100) and c) (001) surfaces. Distances are in Å*

In the (100) surface, the distance between close Ru_{5C} centers is also short (3.137 Å). Nevertheless, the surface morphology avoids the formation of moderate or strong H-bonds between water molecules and OH^-/H^+ moieties. This is a consequence of relative orientation of the $H_w\cdots O_{br}$ and $O_w\cdots H_{br}$ hydrogen bonds with respect to the adjacent water or OH^-/H^+ groups. As a consequence, the adsorption energies are almost invariant to the increase of water coverage both for the *2wat* and *2dpro* situations. Only for the case of the $H_2O_3^-$ dimer formation, cooperative effects seem to be relevant, but in this case, they are not sufficient to overcome the 14.7 kJ mol^{-1} preference for the adsorption of molecular water. Overall, the *2wat* structure is preferred (Figure 6b) but, both the *2wat* and *1wat/1dpro* situations are very close in energy, the difference being less than 1.2 kJ mol^{-1}. This suggests that both situations would be present in this surface and the amount of deprotonated water would be lower than 50%.

Finally, Ru_{5C} centers at the (001) surface are all separated by more than 4 Å. Therefore, no cooperative effects can be established between water molecules, when coverage increases. This turns in adsorption energies that are marginally lower than those of the isolated water molecule. Remarkably with respect to what is found in the smaller coverages, we were able to find a structure in which at least one water molecule deprotonates, but this situation is 3.3 kJ mol^{-1} less favorable than the adsorption of molecular water. Therefore, no deprotonation would occur at the (001) surface, the most favorable structure being represented in Figure 6c.

Overall, at coverages θ = 2/4 and regardless of the surface morphology, the preferred situation implies the adsorption of water molecules in contiguous Ru centers forming H-bond chains. The degree of water deprotonation varies significantly as a function of the considered surface and this is controlled by the strength of the cooperative effects determined by surface

morphology. In the (110) and (011) surfaces, morphology allows the formation of strong cooperative effects, which results in the formation of chains constituted by formal $H_3O_2^-$ dimers leading to a high degree of deprotonation (50%). For the other facets, cooperative effects are weaker and the degree of deprotonation tends to decrease. For instance, the preferred structure of the (100) is the adsorption of water molecules (0% deprotonation), although the structure with 50% of deprotonated water is only marginally less favorable. Finally, the preferred adsorption mode in the (001) surface is molecular water, as a result of a very large distance between Ru centers.

The stronger hydrogen bonding at 50% of deprotonation can be understood by analyzing the variation of the acid and basic strength of the resulting species when interacting with the surface. Adsorbed water becomes more acidic when it interacts with Ru centers (positive Bader atomic charges), and more basic when it deprotonates (the OH fragment is negatively charged). Therefore, the interaction of one adsorbed molecule (acting as donor) with one OH^- species (acting as an acceptor) forms a strong hydrogen bond, leading to the formation of the formal $H_3O_2^-$ dimer. The hydrogen bond is intermediate when the species involved are both water or OH^- species since either the acceptor or the donor is not optimal. The worst situation is the interaction of an OH^- group as a donor and a water molecule as acceptor, which leads to very long hydrogen bonds. This behavior perfectly correlates with the observed trends in H-bonding distances. (*Supporting Information S5).*

Water adsorption at monolayer coverages (θ = (4/4)). With the aim of analyzing the structure of a water monolayer on each surface, we considered the adsorption of four water molecules per unit cell for the (110), (100) and (001) facets and 8 water molecules in the (011) surface. In all cases, the water molecules occupy one unsaturated ruthenium center and this leads to a density of water molecules close to 5 per nm^2 in the (110) and (001) surfaces and between 7

and 8 for the (011) and (100) (see Table 4). For each facet, we started from the situation in which there is no water deprotonation, and successively deprotonate water molecules until deprotonation becomes unfavorable. Table 4 reports the adsorption energies per water molecule, some selected distances, the Bader atomic charges and the adsorption energy per surface area (A^2) of the most favorable degree of deprotonation. The reference conformation consisting in a monolayer without any deprotonation is added for comparison. Figure 7 shows the optimized geometry of the preferred structure in each facet. Further information on the structures and energetics of other water deprotonation degrees can be found in the *Supporting Information (Section S6)*.

The addition of water molecules to the most stable $\theta = 2/4$ coverage structures leads to the formation of a second water chain that it is separated from the initial one by the presence of the O_{br} chain. This results in a significant separation between the two water chains and thus, there is almost no interaction between water molecules of different chains. However, depending on the nature of the O_{br}, the facets can be divided into two groups. In the case of the (110), the O_{br} atoms involved in the hydrogen bonding with the adsorbed water molecules are not bonded to unsaturated Ru centers and thus, the increase of water coverage has very little influence in the relative stabilities of the non-deprotonated and deprotonated adsorption modes. In contrast, for the other surfaces ((011), (100) and (001)), the O_{br} centers are directly bonded to an unsaturated Ru atom that becomes the adsorption center of the additional water molecules. As a consequence, the adsorption energies and preferred structures are influenced by the increase of water coverage, favoring water deprotonation.

In detail, the addition of two water molecules to the $\theta = 2/4$ coverage structures of the (110) leads to the formation of a second chain, which can be formed of either water molecules, $H_3O_2^-$ building blocks or OH^- groups, without any relevant interaction with the first chain. In this context,

the water monolayer without any water dissociation corresponds to a structure formed by two parallel chains of water molecules and the corresponding adsorption energy per water molecule, albeit marginally smaller, is almost that of water adsorption without dissociation with the $\theta = 2/4$ coverage. The most favorable situation corresponds to the dissociation of two water molecules per unit cell (*2dpro*), one in each water chain, so that the resulting structure presents two parallel chains made of the formal $(H_3O_2)^-$ dimer as basic unit. Consequently, the adsorption energy per water molecule resembles that of a single chain of $(H_3O_2)^-$ species. Following the same argumentation, the structure with only one dissociated water molecule corresponds to the situation in which there are alternate water and $(H_3O_2)^-$ parallel chains, with an adsorption energy per water molecule that is in between the adsorption energies of the two chains (water and $(H_3O_2)^-$) separately (-143.0 kJ mol^{-1}). Finally, the structure of 3 dissociated water molecules per unit cell, corresponds to two parallel chains: one has OH^- groups as building blocks and the other is formed by the $(H_3O_2^-)$ units. Results for the $\theta = 2/4$ coverage revealed that the chain with the $(H_3O_2^-)_n$ is preferred over the chain formed by OH^- groups, therefore, the situation with three dissociated water molecules is less favorable than the formation of two $(H_3O_2^-)_n$ chains. Indeed, the associated adsorption energy per water molecule is again in between the values obtained for the two chains separately.

Table 4. *Water adsorption energies on the most favorable facets (in kJ mol^{-1}) at monolayer coverages θ=(4/4 or 8/8) and the associated main geometrical structural parameters (in Å or degrees).*

(h k l)		ρ_{H2O}[a]	E_{ads}	$E_{ads/A}$	d(O_wH_w)	d($O_{br}H_w$)	∠(H_2O)	d(RuO_w)	d(O_wH_{w2})	q_{Obr}[b]	q_{H2O}[b]
(1 1 0) **(4:2)**	*wat*	4.96	-138.0	-27.4	0.981 1.031	1.728	105.9	2.231	2.281	-0.86	+0.08
	dpro	4.96	-147.7	-29.3	0.973 1.524	0.995	106.7	2.131	1.689	-0.71[c] -1.11[d]	0.09[c] -0.40/+0.62[d]
(0 1 1) **(8:4)**	*dpro*	7.97	-130.4	-82.9	0.986 1.034	1.024	106.6	2.096	1.475		
(1 0 0) **(4:1)**	*wat*	7.02	-135.4	-38.0	0.980 1.018	1.587	105.4	2.176	2.245		+0.08
	dpro	7.02	-136.2	-38.2	0.983 1.151	1.023	106.4	2.137	1.750		0.09[c] -0.44/+0.65[d]
(0 0 1) **(4:1)**	*wat*	4.84	-126.9	-24.6	0.984 1.039	1.458	101.1	2.193	2.396		+0.07
	dpro	4.84	-131.0	-25.4	0.975 1.568	1.036	109.4	2.133	1.965		+0.09 -0.57/+0.64

[a] H_2O/nm^2
[b] Average values

The situation is significantly different in the other surfaces. In the (011), (100) and (001) facets, the separating O_{br} chain is formed by oxygen atoms bonded to unsaturated Ru center and the increase of water coverage has an effect both on the adsorption energies and the degree of water deprotonation. In this context, although there is not direct interaction between the water molecules of different chains, the fact that the Ru center bonded to the O_{br} acting as hydrogen-bond acceptor accommodates the adsorption of the additional water molecule produces an important change in the basicity of the O_{br}. Consequently, the $H_w\cdots O_{br}$ becomes stronger, as evidenced by a decrease of the $H_w\cdots O_{br}$ distance of about 0.01 Å and a marginally increase of the

adsorption energy. The increase in the O_{br} basicity also favors the water deprotonation and thus, the amount of deprotonated water tends to increase. These effects are very minor on the (011). The adsorption energy per water molecule on the (011) surface at $\theta = 4/4$ coverages is very similar to that of the half monolayer coverage and the degree of deprotonation remains at 50%. In fact, the major difference with the half monolayer coverage in this (011) facet is that while for $\theta = 2/4$ several different minima were found with different degrees of deprotonation at the monolayer coverages only structures with 50% of deprotonation were achieved. All our attempts to localize structures with higher and lower degrees of deprotonation spontaneously evolved to structures with 4 water and 4 H^+/OH^- units. Regarding the (100) facet, the adsorption energy increases 7.9 kJ mol^{-1} with respect to the $\theta = 2/4$ situation and the associated global minimum presents 25% of deprotonated water molecules instead of 0% as in the preferred structure of the half monolayer coverage. Finally, in the (001) facet, the preferred degree of deprotonation is also 25% and the adsorption energy per water molecule increases from -126.2 kJ mol^{-1} in the $\theta = 2/4$ to -131.0 kJ mol^{-1} in $\theta = 4/4$. All these data were used to determine the most favorable coverage at different temperatures through ab-initio thermodynamics (Supporting Information). Results show that from 0 to around 700 K the preferred coverage is the monolayer and this is regardless of the surface. At around this temperature, water desorption begins, and it does not take place stepwise. Once the monolayer coverage becomes unfavorable the preferred structure becomes the 0 coverage. Although the temperature of desorption may be too high, results suggest a general preference for the monolayer coverage.

Overall, when increasing the water coverage from the most stable structures of the half monolayer situation to the full monolayer, cooperative effects between water molecules remain unchanged. This is due to the formation of parallel water chains that are too far apart for forming

hydrogen bonding interaction between them. However, the increase of O_{br} basicity due to the adsorption of water molecules in unsaturated Ru centers bonded to this O_{br} centers increases the degree of deprotonation and/or the adsorption energy per water molecule in the (100) and (001) surfaces. The final amount of deprotonated water in the monolayer is 50% in the (110) and (011) facets and 25% in the (100) and (001) surfaces. This degree of deprotonation trend within the different facets is in good agreement with results reported in a very recent contribution.[42]

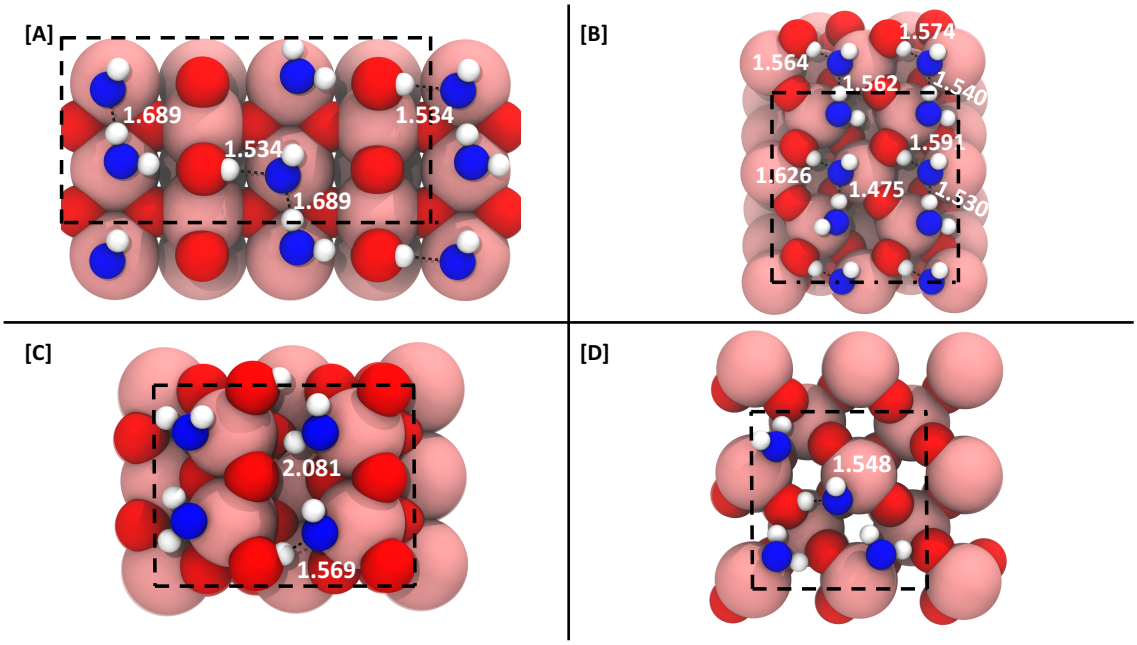

Figure 8. *Optimized geometries of the most stable structures associated to water adsorption with monolayer coverage (θ = 4/4 or 8/8) on the: a) (110); b) (011); c) (100) and d) (001) surfaces. Distances are in Å*

At this point it is worth mentioning that while the adsorption energy per water molecule is an important descriptor for analyzing how strong is the interaction between water and RuO_2 in the interface, other factors are also key. In particular, the density of unsaturated Ru centers on the surface is significantly different in the four studied facets. In fact, the number of water molecules adsorbed per unit area is significantly higher in the (011) and (100) surfaces and thus the adsorption

energy per surface area does not correlate with the strength of the RuO_2-H_2O interaction of each particular water molecule (higher for the (110) surface). Indeed, considering the water density over the surface, the strongest water-RuO_2 surface interaction is observed in the (011) facet, followed by the (100). This suggest that these two surfaces will be the most stabilized ones in solution with respect with their surface energies in vacuum. As a consequence, the Wulff construction (See Figure 3) with the surface energies resulting after considering the H_2O-RuO_2 interface shows that the major facet would be the (011) with small contributions from the (100) and (110) surfaces. Despite the limitations of the current approach this suggest very different nanoparticle shapes depending on the synthetic procedure (vacuum or solution).

Conclusions

Understanding the RuO_2 – water interface and the adsorption of water on the most relevant RuO_2 surfaces is important for characterizing the nature of the surface species that can be involved in the catalytic activity of hydrous RuO_2 in oxidation reactions or in the electrochemical processes. This includes the water oxidation reaction, which is seen as an alternative environmentally friendly source of energy. In this context, we analyzed the influence of water coverage and surface morphology in the adsorption energy per water molecule and the degree of water deprotonation. For that, we considered the four most relevant surfaces non polar ((110), (011), (100) and (001)) and three different coverages: isolated water molecules, half monolayer and the full monolayer. Present results suggest that the water adsorption energy and the degree of deprotonation are controlled by three main factors. The first one is the intrinsic acidity of the unsaturated ruthenium centers and the basicity of the O_{br} groups in the pristine surface. The former increases when decreasing the coordination number of the ruthenium center. The latter is highly influenced by the

energy levels of the p orbitals of the O_{br}, which are related with the Ru-O_{br}-Ru angle. This leads to the fact that deprotonation at very low coverages is only favorable for the (110) surface. The second factor is the presence of cooperative effects between the adsorbed water molecules, which generates a chain of interacting species adsorbed on contiguous ruthenium centers. The usual preferred structure when cooperative effects are important is the formation of the formally $(H_3O_2)^-$ unit that presents a strong internal hydrogen bond. Since the (110) surface is the flattest one and presents short distances between contiguous ruthenium centers, it also presents the strongest cooperative effects, maximizing a degree of deprotonation of the 50%. In contrast, the (001) surface, with the most separated Ru-centers, presents the weakest cooperative effects, the weakest adsorption energies and the smallest degree of deprotonated water. Finally, it has been observed that O_{br} groups become more basic when additional water molecules to the half monolayer structures are adsorbed on Ru centers bonded to these O_{br} groups. This occurs at the highest coverages of the (011), (100) and (001) resulting in stronger adsorption energies and slightly higher water deprotonation percentages when moving from the single chain of adsorbed water molecules to the monolayer. Interestingly, the density of unsaturated ruthenium centers in the different surface varies significantly, thus the interaction energies between water and RuO_2 per surface area do not correlate with the adsorption energies per water molecule leading to a stronger H_2O-RuO_2 interaction for those surfaces with a higher density of defective centers ((011) and (100)) surfaces. Overall, the strength of the water adsorption and the degree of deprotonation (50% for the monolayers of the (110) and (011) but 25% for those of the (100) and (001)) significantly varies as function of the surface morphology. Therefore, the synthesis of materials with one particular predominant face could tune the material properties and, ultimately, could have an influence in the catalytic processes.

The authors declare no competing financial interests

Acknowledgements. The authors gratefully acknowledge financial support from MINECO (CTQ2017-89132-P) and the Generalitat de Catalunya (2014SGR-482). XSM is grateful for the Professor Agregat Serra Húnter position.

Supporting Information. The supporting information including the calibration of the plane wave energy cut-off (Section S1), the calibration of the k-point mesh (Section S2), the calibration of the surface model thickness (Section S3), all optimized structures associated with the adsorption of isolated water molecules (Section S4), half monolayer (Section S5) and full monolayer (Section S6) can be found free of charge at the ACS Publication website.

References

(1) Over, H. Surface Chemistry of Ruthenium Dioxide in Heterogeneous Catalysis and Electrocatalysis: From Fundamental to Applied Research. *Chem. Rev.* **2012**, *112* (6), 3356–3426.

(2) Kuhlenbeck, H.; Shaikhutdinov, S.; Freund, H.-J. Well-Ordered Transition Metal Oxide Layers in Model Catalysis – A Series of Case Studies. *Chem. Rev.* **2013**, *113* (6), 3986–4034.

(3) Hess, F.; Over, H. Rate-Determining Step or Rate-Determining Configuration? The Deacon Reaction over RuO 2 (110) Studied by DFT-Based KMC Simulations. *ACS Catal.* **2017**, *7* (1), 128–138.

(4) Over, H. Atomic-Scale Structure and Catalytic Reactivity of the RuO2(110) Surface. *Science (80-.).* **2000**, *287* (5457), 1474–1476.

(5) Fan, C. Y.; Wang, J.; Jacobi, K.; Ertl, G. The Oxidation of CO on RuO2(110) at Room Temperature. *J. Chem. Phys.* **2001**, *114* (22), 10058–10062.

(6) López, N.; Gómez-Segura, J.; Marín, R. P.; Pérez-Ramírez, J. Mechanism of HCl Oxidation (Deacon Process) over RuO2. *J. Catal.* **2008**, *255* (1), 29–39.

(7) Liu, H.; Iglesia, E. Selective Oxidation of Methanol and Ethanol on Supported Ruthenium Oxide Clusters at Low Temperatures †. *J. Phys. Chem. B* **2005**, *109* (6), 2155–2163.

(8) Teschner, D.; Farra, R.; Yao, L.; Schlögl, R.; Soerijanto, H.; Schomäcker, R.; Schmidt, T.; Szentmiklósi, L.; Amrute, A. P.; Mondelli, C.; et al. An Integrated Approach to Deacon Chemistry on RuO2-Based Catalysts. *J. Catal.* **2012**, *285* (1), 273–284.

(9) Weaver, J. F. Surface Chemistry of Late Transition Metal Oxides. *Chem. Rev.* **2013**, *113* (6), 4164–4215.

(10) Exner, K. S.; Anton, J.; Jacob, T.; Over, H. Controlling Selectivity in the Chlorine Evolution Reaction over RuO 2 -Based Catalysts. *Angew. Chemie Int. Ed.* **2014**, *53* (41), 11032–11035.

(11) Suen, N.-T.; Hung, S.-F.; Quan, Q.; Zhang, N.; Xu, Y.-J.; Chen, H. M. Electrocatalysis for the Oxygen Evolution Reaction: Recent Development and Future Perspectives. *Chem. Soc. Rev.* **2017**, *46* (2), 337–365.

(12) Jung, H.-G.; Jeong, Y. S.; Park, J.-B.; Sun, Y.-K.; Scrosati, B.; Lee, Y. J. Ruthenium-Based Electrocatalysts Supported on Reduced Graphene Oxide for Lithium-Air Batteries. *ACS Nano* **2013**, *7* (4), 3532–3539.

(13) Paoli, E. A.; Masini, F.; Frydendal, R.; Deiana, D.; Schlaup, C.; Malizia, M.; Hansen, T. W.; Horch, S.; Stephens, I. E. L.; Chorkendorff, I. Oxygen Evolution on Well-Characterized Mass-Selected Ru and RuO 2 Nanoparticles. *Chem. Sci.* **2015**, *6* (1), 190–196.

(14) Reier, T.; Oezaslan, M.; Strasser, P. Electrocatalytic Oxygen Evolution Reaction (OER) on Ru, Ir, and Pt Catalysts: A Comparative Study of Nanoparticles and Bulk Materials. *ACS Catal.* **2012**, *2* (8), 1765–1772.

(15) Over, H.; Muhler, M. Catalytic CO Oxidation over Ruthenium - Bridging the Pressure Gap. *Prog. Surf. Sci.* **2003**, *72* (1–4), 3–17.

(16) Reuter, K.; Scheffler, M. First-Principles Kinetic Monte Carlo Simulations for Heterogeneous Catalysis: Application to the CO Oxidation at RuO2(110). *Phys. Rev. B Condens. Matter Mater. Phys.* **2006**, *73* (4), 045433/1-045433/17.

(17) Teschner, D.; Novell-Leruth, G.; Farra, R.; Knop-Gericke, A.; Schlögl, R.; Szentmiklósi, L.; Hevia, M. G.; Soerijanto, H.; Schomäcker, R.; Pérez-Ramírez, J.; et al. In Situ Surface Coverage Analysis of RuO2-Catalysed HCl Oxidation Reveals the Entropic Origin of Compensation in Heterogeneous Catalysis. *Nat. Chem.* **2012**, *4* (9), 739–745.

(18) Trasatti, S. Electrocatalysis: Understanding the Success of DSA®. *Electrochim. Acta* **2000**, *45* (15–16), 2377–2385.

(19) Ling Zang, H. K. Room Temperature Oxidation of CarbonMonoxide Catalyzed by Hydrous RutheniumDioxide. *Angew. Chem. Int. Ed. Commun.* **2000**, *39* (21), 3921.

(20) Rolison, D. R.; Hagans, P. L.; Swider, K. E.; Long, J. W. Role of Hydrous Ruthenium Oxide in Pt–Ru Direct Methanol Fuel Cell Anode Electrocatalysts: The Importance of Mixed Electron/Proton Conductivity. *Langmuir* **1999**, *15* (3), 774–779.

(21) Paulus, U. A.; Wang, Y.; Kim, S. H.; Geng, P.; Wintterlin, J.; Jacobi, K.; Ertl, G. Inhibition of CO Oxidation on RuO[Sub 2](110) by Adsorbed H[Sub 2]O Molecules. *J. Chem. Phys.* **2004**, *121* (22), 11301.

(22) Nellist, M. R.; Laskowski, F. A. L.; Lin, F.; Mills, T. J.; Boettcher, S. W. Semiconductor–Electrocatalyst Interfaces: Theory, Experiment, and Applications in Photoelectrochemical Water Splitting. *Acc. Chem. Res.* **2016**, *49* (4), 733–740.

(23) Henderson, M. A. The Interaction of Water with Solid Surfaces: Fundamental Aspects Revisited. *Surf. Sci. Rep.* **2002**, *46* (1), 1–308.

(24) Grotevendt, A. G. D.; Lummiss, J. A. M.; Mastronardi, M. L.; Fogg, D. E. Ethylene-Promoted versus Ethylene-Free Enyne Metathesis. *J. Am. Chem. Soc.* **2011**, *133* (40), 15918–15921.

(25) Verdaguer, A.; Sacha, G. M.; Bluhm, H.; Salmeron, M. Molecular Structure of Water at Interfaces: Wetting at the Nanometer Scale. *Chem. Rev.* **2006**, *106* (4), 1478–1510.

(26) Campbell, C. T.; Sellers, J. R. V. Enthalpies and Entropies of Adsorption on Well-De Fi Ned Oxide Surfaces : Experimental Measurements. *Chem. Rev.* **2013**, *113*, 4106–4135.

(27) Mu, R.; Zhao, Z.; Dohnálek, Z.; Gong, J. Structural Motifs of Water on Metal Oxide Surfaces. *Chem. Soc. Rev.* **2017**, *46* (7), 1785–1806.

(28) Borgarello, E.; Kiwi, J.; Pelizzetti, E.; Visca, M.; Grätzel, M. Photochemical Cleavage of Water by Photocatalysis. *Nature* **1981**, *289* (5794), 158–160.

(29) Zhao, Z.; Li, Z.; Zou, Z. Understanding the Interaction of Water with Anatase TiO2 (101) Surface from Density Functional Theory Calculations. *Phys. Lett. A* **2011**, *375* (32), 2939–2945.

(30) Gala, F.; Agosta, L.; Zollo, G. Water Kinetics and Clustering on the (101) TiO2 Anatase Surface. *J. Phys. Chem. C* **2016**, *120* (1), 450–456.

(31) Zhao, Z.-J.; Li, Z.; Cui, Y.; Zhu, H.; Schneider, W. F.; Delgass, W. N.; Ribeiro, F.; Greeley, J. Importance of Metal-Oxide Interfaces in Heterogeneous Catalysis: A Combined DFT, Microkinetic, and Experimental Study of Water-Gas Shift on Au/MgO. *J. Catal.* **2017**, *345*, 157–169.

(32) Lobo, A.; Conrad, H. Interaction of H2O with the RuO2(110) Surface Studied by HREELS and TDS. *Surf. Sci.* **2003**, *523* (3), 279–286.

(33) Chu, Y. S.; Lister, T. E.; Cullen, W. G.; You, H.; Nagy, Z. Commensurate Water Monolayer at the <math Display="inline"> <mrow> <msub> <mrow> <mi>RuO</Mi> </Mrow> <mrow> <mn>2</Mn> </Mrow> </Msub> </Mrow> <mo>(</Mo> <mn>110</Mn>

<mo>)</Mo> </Math> /Water Interface. *Phys. Rev. Lett.* **2001**, *86* (15), 3364–3367.

(34) Rao, R. R.; Kolb, M. J.; Halck, N. B.; Pedersen, A. F.; Mehta, A.; You, H.; Stoerzinger, K. A.; Feng, Z.; Hansen, H. A.; Zhou, H.; et al. Towards Identifying the Active Sites on RuO 2 (110) in Catalyzing Oxygen Evolution. *Energy Environ. Sci.* **2017**, *10* (12), 2626–2637.

(35) Mu, R.; Cantu, D. C.; Glezakou, V.-A.; Lyubinetsky, I.; Rousseau, R.; Dohnálek, Z. Deprotonated Water Dimers: The Building Blocks of Segmented Water Chains on Rutile RuO 2 (110). *J. Phys. Chem. C* **2015**, *119* (41), 23552–23558.

(36) Mu, R.; Cantu, D. C.; Lin, X.; Glezakou, V.-A.; Wang, Z.; Lyubinetsky, I.; Rousseau, R.; Dohnálek, Z. Dimerization Induced Deprotonation of Water on RuO 2 (110). *J. Phys. Chem. Lett.* **2014**, *5* (19), 3445–3450.

(37) Nguyen, M.-T.; Mu, R.; Cantu, D. C.; Lyubinetsky, I.; Glezakou, V.-A.; Dohnálek, Z.; Rousseau, R. Dynamics, Stability, and Adsorption States of Water on Oxidized RuO 2 (110). *J. Phys. Chem. C* **2017**, *121* (34), 18505–18515.

(38) Keilbart, N.; Okada, Y.; Feehan, A.; Higai, S.; Dabo, I. Quantum-Continuum Simulation of the Electrochemical Response of Pseudocapacitor Electrodes under Realistic Conditions. *Phys. Rev. B* **2017**, *95* (11), 115423.

(39) Siahrostami, S.; Vojvodic, A. Influence of Adsorbed Water on the Oxygen Evolution Reaction on Oxides. *J. Phys. Chem. C* **2015**, *119* (2), 1032–1037.

(40) Wirth, J.; Monturet, S.; Klamroth, T.; Saalfrank, P. Adsorption and (Photo-) Electrochemical Splitting of Water on Rutile Ruthenium Dioxide. *EPL (Europhysics Lett.* **2011**, *93* (6), 68001.

(41) Wang, Y.; Jacobi, K.; Schöne, W.-D.; Ertl, G. Catalytic Oxidation of Ammonia on RuO 2

(110) Surfaces: Mechanism and Selectivity. *J. Phys. Chem. B* **2005**, *109* (16), 7883–7893.

(42) Rao, R. R.; Kolb, M. J.; Hwang, J.; Pedersen, A. F.; Mehta, A.; You, H.; Stoerzinger, K. A.; Feng, Z.; Zhou, H.; Bluhm, H.; et al. Surface Orientation Dependent Water Dissociation on Rutile Ruthenium Dioxide. *J. Phys. Chem. C* **2018**, *122* (31), 17802–17811.

(43) Kohn, W.; Sham, L. J. Self-Consistent Equations Including Exchange and Correlation Effects. *Phys. Rev.* **1965**, *140* (4A).

(44) Kresse, G.; Hafner, J. Ab Initio Molecular Dynamics for Liquid Metals. *Phys. Rev. B* **1993**, *47* (1), 558–561.

(45) Kresse, G.; Furthmüller, J. Efficient Iterative Schemes for Ab Initio Total-Energy Calculations Using a Plane-Wave Basis Set. *Phys. Rev. B* **1996**, *54* (16), 11169–11186.

(46) Blöchl, P. E. Projector Augmented-Wave Method. *Phys. Rev. B* **1994**, *50* (24), 17953–17979.

(47) Kresse, G.; Joubert, D. From Ultrasoft Pseudopotentials to the Projector Augmented Wave Method. *Phys. Rev. B* **1999**, *59* (3), 1758–1775.

(48) Perdew, J. P.; Burke, K.; Ernzerhof, M. Generalized Gradient Approximation Made Simple. *Phys. Rev. Lett.* **1996**, *77*, 3865–3868.

(49) D. Kim, H.-S.; Yang, J.; Qi, Y.; Rappe, A. M. Adsorption of Benzene on the RuO 2 (110) Surface. *J. Phys. Chem. C* **2017**, *121* (3), 1585–1590.

(50) Li, T.; Rai, R.; Liang, Z.; Kim, M.; Asthagiri, A.; Weaver, J. F. Adsorption and Oxidation of n -Butane on the Stoichiometric RuO 2 (110) Surface. *J. Phys. Chem. C* **2016**, *120* (18), 9863–9873.

(51) Grimme, S. Accurate Description of van Der Waals Complexes by Density Functional Theory Including Empirical Corrections. *J. Comput. Chem.* **2004**, *25* (12), 1463–1473.

(52) Monkhorst, H.; Pack, J. Special Points for Brillouin Zone Integrations. *Phys. Rev. B* **1976**, *13* (12), 5188–5192.

(53) Ugliengo, P.; Viterbo, D.; Chiari, G. MOLDRAW: Molecular Graphics on a Personal Computer. *Zeitschrift fur Krist. - New Cryst. Struct.* **1993**, *207* (Part-1), 9–23.

(54) Henkelman, G.; Uberuaga, B. P.; Jónsson, H. Climbing Image Nudged Elastic Band Method for Finding Saddle Points and Minimum Energy Paths. *J. Chem. Phys.* **2000**, *113* (22), 9901–9904.

(55) Henkelman, G.; Jónsson, H. Improved Tangent Estimate in the Nudged Elastic Band Method for Finding Minimum Energy Paths and Saddle Points. *J. Chem. Phys.* **2000**, *113* (22), 9978–9985.

(56) Sheppard, D.; Terrell, R.; Henkelman, G. Optimization Methods for Finding Minimum Energy Paths. *J. Chem. Phys.* **2008**, *128* (13).

(57) Huang, Y. S.; Park, H. L.; Pollak, F. H. Growth and Characterization of RuO2 Single Crystals. *Mater. Res. Bull.* **1982**, *17* (10), 1305–1312.

(58) Baur, W. H.; Khan, A. A. Rutile-Type Compounds. IV. SiO2, GeO2 and a Comparison with Other Rutile-Type Structures. *Acta Crystallogr. Sect. B Struct. Crystallogr. Cryst. Chem.* **1971**, *27* (11), 2133–2139.

(59) Kim, Y. D.; Over, H.; Krabbes, G.; Ertl, G. Identification of RuO2 as the Active Phase in CO Oxidation on Oxygen-Rich Ruthenium Surfaces. *Top. Catal.* **2000**, *14* (1), 95–100.

(60) Kim, Y. D.; Schwegmann, S.; Seitsonen, A. P.; Over, H. Epitaxial Growth of RuO 2 (100) on Ru(101¯0): Surface Structure and Other Properties. *J. Phys. Chem. B* **2001**, *105* (11), 2205–2211.

(61) Seitsonen, A. P.; Over, H. Ruthenium Dioxide, a Versatile Oxidation Catalyst: First Principles Analysis. In *High Performance Computing in Science and Engineering, Munich 2002: Transactions of the First Joint HLRB and KONWIHR Status and Result Workshop, October 10--11, 2002, Technical University of Munich, Germany*; Wagner, S., Bode, A., Hanke, W., Durst, F., Eds.; Springer Berlin Heidelberg: Berlin, Heidelberg, 2003; pp 177–187.

(62) Novell-Leruth, G.; Carchini, G.; López, N. On the Properties of Binary Rutile MO 2 Compounds, M = Ir, Ru, Sn, and Ti: A DFT Study. *J. Chem. Phys.* **2013**, *138* (19), 194706.

(63) Wulff, G. Zur Frage Der Geschwindigkeit Des Wachstums Und Der Auflösung Der Krystallflächen. *Zeitschrift für Kryst. und Mineral.* **1901**, *34*, 449–530.

(64) Ong, S. P.; Richards, W. D.; Jain, A.; Hautier, G.; Kocher, M.; Cholia, S.; Gunter, D.; Chevrier, V. L.; Persson, K. A.; Ceder, G. Python Materials Genomics (Pymatgen): A Robust, Open-Source Python Library for Materials Analysis. *Comput. Mater. Sci.* **2013**, *68*, 314–319.

(65) All Attempts to Optimize a Deprotonated Structure from the Species with Two Hydrogen Bonds Collapsed to the Non-Deprotonated One.

(66) A Second Structure in Which the Protonated O2C Atoms Belong to the Same Row Is Also a Minimum of the Potential Energy Surface, but Its Adsorption Energy Is Smaller (-141.7 Kcal Mol-1).